Mutual Inductance Calculation of Movable Planar Coils on Parallel Surfaces

Y. P. Su, *Student Member, IEEE*, Xun Liu, *Member, IEEE*, and S. Y. Ron Hui, *Fellow, IEEE*

***Abstract*—Recent developments of the wireless battery charging platform have prompted requirements to investigate the mutual inductance between a movable planar coil and the fixed planar coil on the charging platform. The wireless battery charging platform must allow the load to be placed anywhere on the charging surface. Therefore, the relative position between the movable energy-receiving coil and the energy-transmitting coils on the charging platform must be flexible. In this paper, an extended formula is proposed for the mutual inductance calculation for two coaxial or noncoaxial planar spiral windings sandwiched between two *double-layer* substrates. It can quickly determine the mutual coupling of two planar windings that can have different relative positions and distance between them. This new calculation method provides a new and useful tool for determining the mutual inductance of a movable planar coil and the fixed planar coil on the wireless battery charging platform. The theory has been favorably tested and compared with practical measurements and also with finite-element analysis.**

***Index Terms*—Contactless battery charging platform, impedance formula, noncoaxial, planar spiral inductor.**

NOMENCLATURE

d	Distance between axis of primary winding and axis of secondary winding.
d_1, d_2 , d_1', d_2'	Illustrated in Fig. 2 .
$f(\lambda)$, $g(\lambda)$	Defined in (13) and (14).
h_1, h_2	Windings heights in axial direction for primary winding and secondary winding.
$J_1(x)$, $J_0(x)$	Bessel functions of the first kind.
M	Mutual inductance between two windings or filaments in air.
$M_{\rm co}$	Mutual inductance between two coaxial windings.
R_{P1}, R_{S1}	Internal radius of windings.
R_{P2}, R_{S2}	External radius of windings.
R_P, R_S	Radius of filamentary turns.
S	Substrates separation in sandwich structure.
t_1, t_2 , t_3, t_4	Substrate thickness illustrated in Fig. 2.
Z	Mutual impedance between two windings or filaments.
Z_c^f , Z_c^p	Additional mutual impedance due to sandwich structure for coaxial filaments and windings, respectively.
$Z_{\rm nc}^f$, $Z_{\rm nc}^p$	Additional mutual impedance due to sandwich structure for noncoaxial filaments and windings, respectively.
$\lambda(t_1,t_2)$, $\lambda(t_3,t_4)$	Defined in (3) and (4).
μ_0	Permeability of free space $4\pi \times 10^{-7}$ H/m.
μ_{r1}, μ_{r2}	Relative permeability of the substrates.
σ_1, σ_2	Electrical conductivity of the substrates.
ω	Angular frequency (radians per second).

Manuscript received July 17, 2008; revised October 13, 2008. First published March 27, 2009; current version published nulldate. This work was supported by the Hong Kong Research Grant Council under Competitive Earmarked Research Grant (CERG) Project CityU 114105 and by the City University of Hong Kong under Strategic Research Grant 7001761. Recommended for publication by Associate Editor B. Ferreira.

Y. P. Su and S. Y. R. Hui are with the Center for Power Electronics, Department of Electronic Engineering, City University of Hong Kong, Kowloon, Hong Kong (e-mail: eeronhui@cityu.edu.hk).

X. Liu is with the ConvenientPower HK, Ltd., Shatin, NT, Hong Kong (e-mail: xun.liu@convenientpower.com).

Color versions of one or more of the figures in this paper are available online at http://ieeexplore.ieee.org.

Digital Object Identifier 10.1109/TPEL.2008.2009757

I. INTRODUCTION

BASED on the fundamental principle of electromagnetism, the "contactless" transformer makes use of high-frequency alternating magnetic field to transfer power from a primary winding (transmitter) to a secondary winding (receiver). Contactless energy transmission systems (CETSs) are suitable for applications in small power electrical chargers, such as electric shavers, electric toothbrushes, or mobile phones [1]–[3]. However, in the traditional contactless charging systems, the loads must be placed in specific locations for effective energy transfer. Other wireless techniques for transmitting both power and signal for implantable medical devices are reported in [4] and [5]. The transcutaneous transmission of energy

for medical implants can substantially improve the quality of life of the patients, because the batteries of the implants can be recharged and do not have to be replaced frequently. For high-power density and slim-design consideration, the printed circuit board (PCB) planar spiral inductors are preferred in these applications. The mutual coupling between transmitter windings and receiver windings is a very important parameter in the contactless power charging system design, which determines the contactless power transmission capacity and efficiency.

For consumer electronic products, the wide variety of battery chargers has posed a rising concern on the electronic waste problem. It is estimated that over 1.8 billion chargers were made for portable consumer electronic products in 2007. The need for unifying the charging protocol for a wide range of portable electronic products becomes imminent. One attractive solution is the use of CETSs. According to the direction of the magnetic flux used for inductive coupling, CETSs can be divided into three categories. The first method uses 3-D windings to transmit and/or receive magnetic flux, which was proposed by Baarman *et al.* [6]–[12]. It has found applications in water treatment systems and lamp assembly where the system (transmitter and/or receiver) normally occupies large volume. The second approach generates horizontal flux flowing in parallel with the charging surface [13], [14]. To effectively couple with the generated flux, the cross section of the receiver winding must be large (wide and thick) enough, which may not be favored by the slim design of modern mobile electronic devices. The third group includes the approaches generating vertical flux. With the help of the shielded structure, the magnetic flux flows in and out of the charging surface like a water fountain [15]–[17]. The vertical flux is beneficial to the slim design of the receiver windings because the energy transfer takes place on its whole area. In addition, energy transfer can be enclosed and shielded within the contact area between the electronic device and the charging surface of the charging platform. Some fundamental research of a low-profile planar universal contactless battery charging platform has been reported in [18]–[21] in order to improve the convenience and user-friendliness of contactless charging systems. Preferably, the proposed charging system should allow a plurality of products to be charged simultaneously, regardless of their positions and orientations on the charging surface.

With new developments such as the universal wireless battery charging platform, it is necessary to investigate the mutual inductance between a movable energy-receiving coil and the planar energy-transmitting windings on the charging surface. A set of theories that are used to calculate the mutual inductance of two planar coaxial coils: 1) in air; 2) on a single-layer substrate; and 3) sandwiched between two single-layer substrates have been presented in [22]–[24] by the research team at the National University of Ireland, Galway, Ireland. The electromagnetic (EM) shield can affect the magnetic flux distribution, and thus, must be included in the mutual inductance calculation. Similar structures have also been analyzed by current image method in [25] and [26]. Furthermore, these theories have been extended to cover planar coils with an effective *double-layer* EM shield [27], [28]. It must be noted that all the earlier analyses

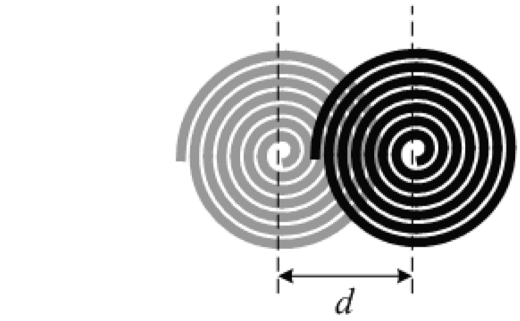

(a)

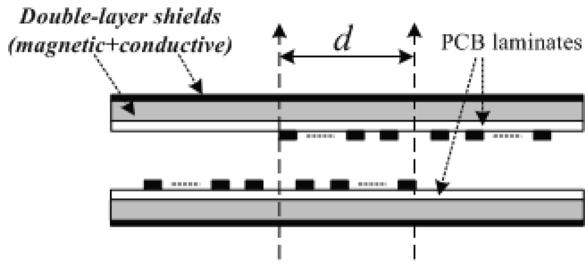

(b)

Fig. 1. Two noncoaxial circular spiral windings. (a) Top view without shields. (b) Cross-sectional view with double-layer shields.

were carried out on the basis that the primary and secondary planar coils for wireless energy transfer are coaxial.

In practice, the wireless battery charging platform may allow the load to be placed anywhere on the charging surface. So the energy-transmitting coils and energy-receiving coils are most likely in a noncoaxial position. Two noncoaxial circular planar spiral windings sandwiched in double-layer EM shields are presented in Fig. 1, with (a) top view and (b) cross-sectional view. The shielding structures are not included in Fig. 1(a) for clarity. In this paper, a generalized theory based on the analytical method in [22] and [23] has been developed to calculate the mutual inductance of circular planar spiral windings sandwiched between double-layer planar EM shields for both coaxial and noncoaxial cases. Using the formula presented, the mutual inductance of two coaxial or noncoaxial planar spiral windings can be determined directly and quickly, without using the time-consuming finite-element analysis (FEA). Calculated results are favorably compared with the finite-element simulation results and practical measurements in a case study. Some analysis is also presented, which leads to some interesting findings.

II. Formula Derivation

A set of frequency-dependent impedance formulas for planar spiral windings on a magnetic substrate of finite thickness or planar coils sandwiched between two magnetic substrates are described in [23], which considers the nonuniform current distribution in planar coils and the power loss in magnetic media. The general procedure for solving the Maxwell's equation in this class of problems has also been outlined in [23]. In this

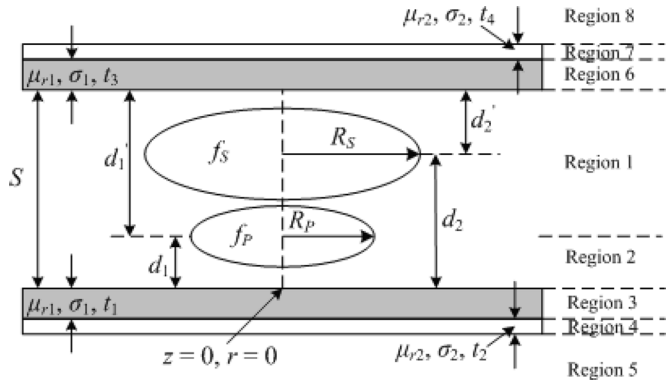

Fig. 2. Filamentary turns sandwiched between two double-layer substrates.

paper, such technique is extended to planar spiral coils sandwiched with double-layer shielding structure.

Following a similar analytical procedure in [23], the case of the filamentary turns must be considered first in order to obtain the mutual inductance formula of the planar spiral windings. Fig. 2 shows the structural configuration of two coaxial filamentary turns sandwiched between two double-layer substrates. In the cylindrical coordinates, the primary filament (f_P) at $z = d_1$ and $r = R_P$ carries a sinusoidal current $i_\phi = I_\phi e^{j\omega t}$. The space is divided into eight distinct regions, as shown in Fig. 2, and the Maxwell's equation for each region must be considered respectively. With the help of the Fourier–Bessel integral transformation [29] and boundary conditions, the electric field E_1^* in region 1 in which we are particularly interested is obtained as

$$E_1^*(r,z) = -\frac{1}{2} j\omega\mu_0 I_\phi R_P \int_0^\infty J_1(kr) J_1(kR_P) f(z) dk \quad (1)$$

where J_1 is Bessel function of the first kind and $f(z)$ is a factor determined by the sandwiched substrates structure and the relative position of two turns expressed in (2), as shown at the bottom of this page.

Other functions in (2) are expressed as follows:

$$\lambda(t_1,t_2) = \frac{\phi_1(k) + (\theta(t_2) - m/\theta(t_2) + m) e^{-2\eta_1 t_1}}{1 + \phi_1(k)(\theta(t_2) - m/\theta(t_2) + m) e^{-2\eta_1 t_1}} \quad (3)$$

$$\lambda(t_3,t_4) = \frac{\phi_1(k) + (\theta(t_4) - m/\theta(t_4) + m) e^{-2\eta_1 t_3}}{1 + \phi_1(k)(\theta(t_4) - m/\theta(t_4) + m) e^{-2\eta_1 t_3}} \quad (4)$$

where m, $\theta(t_i)$, $\phi_1(k)$, and $\phi_2(k)$ are defined in (5), (6), (7), and (8), respectively

$$m = \frac{\mu_{r1}\eta_2}{\mu_{r2}\eta_1} \quad (5)$$

$$\theta(t_i) = \frac{1 - \phi_2(k) e^{-2\eta_2 t_i}}{1 + \phi_2(k) e^{-2\eta_2 t_i}} \quad (6)$$

$$\eta_1 = \sqrt{k^2 + j\omega\mu_{r1}\mu_0\sigma_1} \quad (7)$$

$$\eta_2 = \sqrt{k^2 + j\omega\mu_{r2}\mu_0\sigma_2} \quad (8)$$

and

$$\phi_1(k) = \frac{\mu_{r1} - (\eta_1/k)}{\mu_{r1} + (\eta_1/k)} \quad (9)$$

$$\phi_2(k) = \frac{\mu_{r2} - (\eta_2/k)}{\mu_{r2} + (\eta_2/k)}. \quad (10)$$

The derivation of E_1^* can be found in [23].

The electric field for any point of the secondary filament (f_S) at $z = d_2$ and $r = R_S$ can be expressed as

$$\begin{aligned} E_1^*(R_S,d_2) &= -\frac{1}{2} j\omega\mu_0 I_\phi R_P \int_0^\infty J_1(kR_S) J_1(kR_P) f(d_2) dk \\ &= -\frac{1}{2} j\omega\mu_0 I_\phi R_P \int_0^\infty J_1(kR_S) J_1(kR_P) \\ &\quad \times [e^{-k|d_2 - d_1|} + f(\lambda) + g(\lambda)] dk \end{aligned} \quad (11)$$

where

$$f(\lambda) = \frac{\lambda(t_1,t_2) e^{-k(d_2+d_1)} + \lambda(t_3,t_4) e^{-k(d_2'+d_1')}}{1 - \lambda(t_1,t_2)\lambda(t_3,t_4) e^{-2ks}} \quad (12)$$

$$g(\lambda) = \frac{2\lambda(t_1,t_2)\lambda(t_3,t_4) e^{-2ks} \cosh[k(d_2 - d_1)]}{1 - \lambda(t_1,t_2)\lambda(t_3,t_4) e^{-2ks}} \quad (13)$$

and the induced voltage $V = ZI_\Phi$ in f_S due to the source at $z = d_1$ and $r = R_P$ is the loop integral of electric field E_1^*

$$V = -\oint E_1^*(R_S,d_2) dl = -\int_0^{2\pi} E_1^*(R_S,d_2) R_S d\phi. \quad (14)$$

Therefore, the mutual impedance between these two filamentary turns can be readily obtained by $Z = V/I_\Phi$.

A. Two Coaxial Filamentary Turns

For the case of two coaxial circular turns, the electric field in the circular path of the secondary turn is a vector $E_1^*(R_S,d_2)$ that has a constant magnitude independent on ϕ and its direction is always along $\overrightarrow{dl}$. Thus, the loop integral of electric field in (11) can be simplified as

$$V = -\int_0^{2\pi} E_1^*(R_S,d_2) R_S d\phi = -2\pi R_S E_1^*(R_S,d_2) = ZI_\phi. \quad (15)$$

$$f(z) = e^{-k|z-d_1|} + \frac{\lambda(t_1,t_2) e^{-k(z+d_1)} + 2\lambda(t_1,t_2)\lambda(t_3,t_4) e^{-2ks} \cosh\, k(z-d_1) + \lambda(t_3,t_4) e^{-k(s-z+d_1')}}{1 - \lambda(t_1,t_2)\lambda(t_3,t_4) e^{-2ks}}. \quad (2)$$

The mutual impedance between these two coaxial filamentary turns can be obtained as

$$Z = j\omega M + Z_c^f \tag{16}$$

where M is the mutual inductance that would exist in the absence of the substrate and can be calculated by (17), and Z_c^f is the additional impedance due to the presence of the double-layer sandwiched substrates and can be calculated by (18). The real part of Z_c^f, the resistive component, represents the losses due to the eddy currents in the substrates, and the imaginary part of Z_c^f represents the additional inductive reactance enhanced by the substrates

$$M = \mu_0 \pi R_P R_S \int_0^\infty J_1(kR_P) J_1(kR_S) e^{-k|d_2-d_1|} dk \tag{17}$$

$$Z_c^f = j\omega\mu_0 \pi R_P R_S \int_0^\infty J_1(kR_P) J_1(kR_S) [f(\lambda)+g(\lambda)] dk. \tag{18}$$

Compared with the theory in [23], the formulas for double-layer substrates almost have the same format as that for single-layer substrates, except that the parameter functions $f(\lambda)$ and $g(\lambda)$ have been modified into the forms of (12) and (13).

The mutual inductance between two planar windings is obtained in the expression of (19)–(23), by integrating (16) –(18) over the cross section of the conductor in the same manner as in [23]. The current density distribution is taken into account and the variation over the height of the cross section is assumed to be negligible

$$Z = j\omega M + Z_c^p \tag{19}$$

$$M = \frac{\mu_0 \pi}{h_1 h_2 \ln(R_{P2}/R_{P1}) \ln(R_{S2}/R_{S1})} \int_0^\infty S(kR_{P2}, kR_{P1}) \times S(kR_{S2}, kR_{S1}) Q(kh_1, kh_2) e^{-k|d_2-d_1|} dk \tag{20}$$

$$Z_c^p = \frac{j\omega\mu_0 \pi}{h_1 h_2 \ln(R_{P2}/R_{P1}) \ln(R_{S2}/R_{S1})} \int_0^\infty S(kR_{P2}, kR_{P1}) \times S(kR_{S2}, kR_{S1}) [f(\lambda)+g(\lambda)] Q(kh_1, kh_2) dk \tag{21}$$

where

$$Q(kx,ky) \times \begin{cases} = \dfrac{2}{k^2}\left[\cosh k\dfrac{x+y}{2} - \cosh k\dfrac{x-y}{2}\right], & z > \dfrac{h_1+h_2}{2} \\ = \dfrac{2}{k}\left(h + \dfrac{e^{-kh}-1}{k}\right), & z = 0, \quad x = y = h \end{cases} \tag{22}$$

$$S(kx,ky) = \frac{J_0(kx) - J_0(ky)}{k}. \tag{23}$$

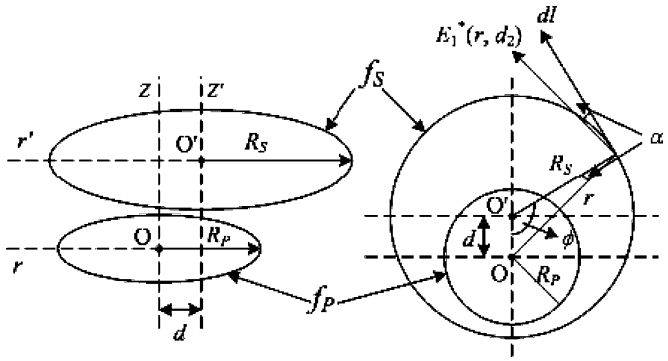

Fig. 3. Two noncoaxial circular filamentary turns.

The variables $f(\lambda)$ and $g(\lambda)$ are defined in (12) and (13).

B. Two Noncoaxial Filamentary Turns

For the case of two noncoaxial circular turns, the electric field in the circular path of the secondary turn is a vector $E_1^*(r, d_2)$. It is a variable, the magnitude and direction of which are highly dependent on ϕ. Unlike the coaxial case, the loop integral of the electric field is more complicated. Fig. 3 illustrates the 3-D view and the top view of two noncoaxial filamentary turns, while the substrates are excluded for a clear view. The induced voltage in f_S by the current source in f_P can be expressed as

$$V = -\oint E_1^*(r, d_2) dl = -\oint E_1^*(r, d_2) dl \cos\alpha. \tag{24}$$

By substituting $\cos\alpha = (R_S - d\cos\phi)/r$ and $dl = R_S d\phi$ into (24)

$$V = -\oint E_1^*(r, d_2) \cos\alpha dl = -\int_0^{2\pi} E_1^*(r, d_2) \frac{R_S - d\cos\phi}{r} R_S d\phi \tag{25}$$

where $r = \sqrt{R_S^2 + d^2 - 2R_S d\cos\phi}$.

So the mutual impedance between these two noncoaxial turns could be acquired as (26). Equation (26) also can be transformed into the format of $Z = j\omega M + Z_{\rm nc}^f$, in which M and $Z_{\rm nc}^f$ are defined as

$$Z = j\omega\mu_0 R_S R_P \int_0^\infty \int_0^\pi \frac{R_S - d\cos\phi}{r} J_1(kr) J_1(kR_P) \times [e^{-k|d_2-d_1|} + f(\lambda) + g(\lambda)] d\phi dk \tag{26}$$

$$M = \mu_0 R_P R_S \int_0^\infty \int_0^\pi \frac{R_S - d\cos\phi}{r} J_1(kR_P) J_1(kr) \times e^{-k|d_2-d_1|} d\phi dk \tag{27}$$

$$Z_{\rm nc}^f = j\omega\mu_0 R_P R_S \int_0^\infty \int_0^\pi \frac{R_S - d\cos\phi}{r} J_1(kR_P) J_1(kr) \times [f(\lambda)+g(\lambda)] d\phi dk. \tag{28}$$

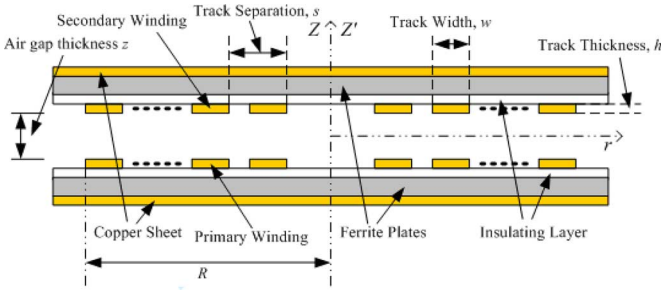

Fig. 4. Cross-sectional view of the prototype in R–Z plane when $d = 0$.

TABLE I
GEOMETRIC PARAMETERS OF THE WINDINGS AND SANDWICH STRUCTURE

Geometric Parameters	Dimension
Copper Track Width, w	0.5*mm*
Copper Track Separation, s	0.8*mm*
Copper Track Thickness, h	140μm
Primary Outmost Radius, R_P	15*mm*
Secondary Outmost Radius, R_S	15*mm*
Number of Primary Turns	6
Number of Secondary Turns	6
Insulating Layer Thickness	0.8*mm*
Ferrite Plate Thickness, t_1, t_3	1*mm*
Copper sheet Thickness, t_2, t_4	0.06*mm*

Applying the same formula transformation from filaments to coils, mutual inductance between two noncoaxial windings is given as

$$Z = j\omega M + Z_{\text{nc}}^{p} \tag{29}$$

$$M = \frac{\mu_0}{h_1 h_2 \ln(R_{P2}/R_{P1}) \ln(R_{S2}/R_{S1})} \times \int_0^{\infty} S(kR_{P1}, kR_{P2})\, Q(kh_1, kh_2)\, e^{-k|d_2 - d_1|} \times \left(\int_0^{\pi} \int_{R_{S1}}^{R_{S2}} \frac{R_S - d\cos\phi}{r} J_1(kr) dR_S d\phi \right) dk \tag{30}$$

$$Z_{\text{nc}}^{p} = \frac{j\omega\mu_0}{h_1 h_2 \ln(R_{P2}/R_{P1}) \ln(R_{S2}/R_{S1})} \times \int_0^{\infty} S(kR_{P1}, kR_{P2})\, Q(kh_1, kh_2) [f(\lambda) + g(\lambda)] \times \left(\int_0^{\pi} \int_{R_{S1}}^{R_{S2}} \frac{R_S - d\cos\phi}{r} J_1(kr) dR_S d\phi \right) dk. \tag{31}$$

III. VERIFICATION

A. Test Conditions

To evaluate the validity of the formula presented, a prototype shown in Fig. 4 is chosen as a practical example. The geometric and characteristic parameters of the planar spiral windings and the sandwich shielding structure are given in Table I. The primary and secondary windings are manufactured on PCB with the identical dimensional parameters, whose photos are shown in Fig. 5. In order to achieve good shielding effectiveness, the material of the two layers of the substrate is assumed to be made of ferrite ($\mu_r = 1000$, $\sigma = 0.1$) and copper ($\mu_r = 0.9999$, $\sigma = 5.8\text{e}7$). It is known that ferrite material is brittle, especially when it is fabricated into thin plates. Limited by the manufacturing process, ferrite manufacturers usually have a maximum area limit for a certain given thickness for their ferrite products. For example, a ferrite product manufacturer may reliably handle ferrite plates of a maximum area of 35 mm × 35 mm for a thickness of 1 mm. If the thickness is reduced, the allowable maximum size will shrink. In this paper, many small ferrite plates are used to form a large ferrite plate in the bottom of the wireless charging platform. During the assembly, the air gap between adjacent ferrite plates has to be minimized in order to reduce the leakage flux. This arrangement can easily be achieved because the ferrite plates have regular (square or rectangular) shapes. In Section II, the analytical model is based on the assumption that the double-layer substrate is infinite in the radial direction. In practice, it is found that as long as the outermost radius (for the circular plate) or the width (for the rectangle plate) of the substrate is twice as large as the outermost radius of the circular winding, the flux leakage due to the fringing effect of the plate can be minimized to a negligible value, and the substrates can be regarded to be infinite compared with the winding size. In the inductance measurement, the used ferrite plate has a dimension of 70 mm × 70 mm, which is constructed by combining four pieces of 35 mm × 35 mm ferrite plates together, all with the thickness of 1 mm.

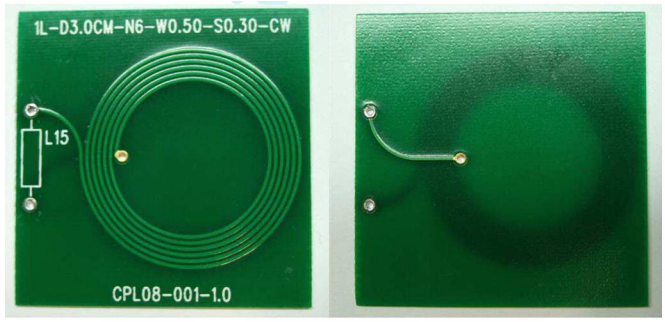

(a) (b)

Fig. 5. Photo of the tested PCB planar spiral winding. (a) Top side. (b) Bottom side.

To obtain the mutual inductance of the prototype, the measurement that involves two stages is performed with the use of an HP4194A impedance analyzer. The measured results are compared with the results from FEA simulation (Ansoft) and calculation (MATLAB). In the first stage, the input impedance of the prototype device is measured in the form of equivalent R_X and L_X , when primary winding and secondary winding are connected in series as the manner shown in Fig. 6(a). Second, the input impedance measurement is carried out when the connection manner between primary winding and secondary winding is changed to that shown in Fig. 6(b). Another equivalent R_Y

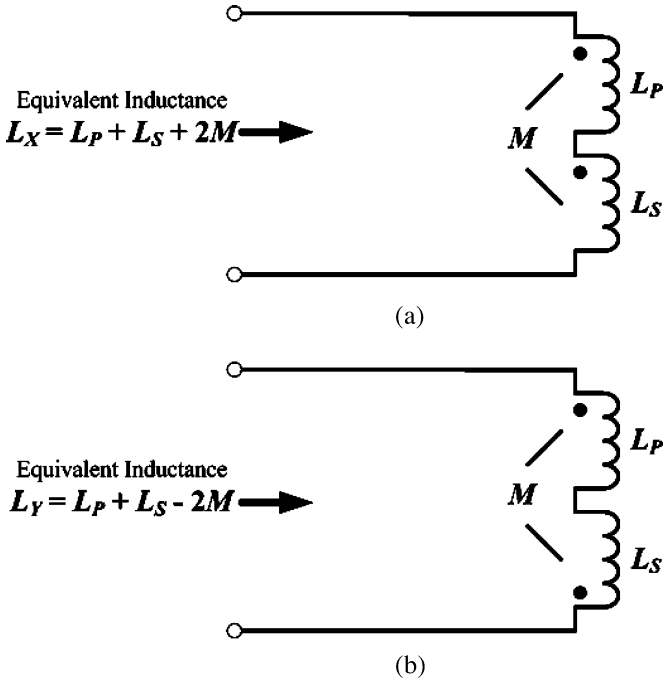

Fig. 6. Two different connection manners between windings in the measurement.

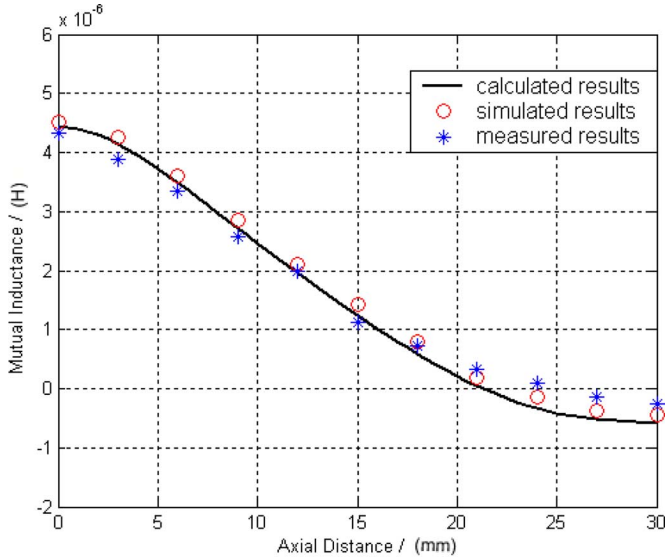

Fig. 7. Mutual inductance as a function of axial distance.

and L_Y can be obtained from this stage. Then the mutual inductance M can be calculated with the use of

$$M = \frac{L_X - L_Y}{4}. \tag{32}$$

The influence of the double-layer EM shield on the windings' inductance has been analyzed in [28]. It has been shown that the negative effect of the conductive layer on both inductance and the eddy current in the conductive layer is negligible, if the thickness of magnetic layers is beyond a critical value. In this paper, the analysis is focused on the mutual inductance between two noncoaxial planar windings, where the axial distance d or the air gap thickness z can change, in order to investigate the effect of the windings' relative positions on the windings' mutual inductance. The operating frequency is fixed at 500 kHz in this study, which is a typical working frequency of the contactless charging platform.

B. Variation of the Axial Distance d

In the first test, the axial distance d is changed from 0 to 30 mm in several steps, while other parameters are kept constant and the air gap z is fixed at 2 mm. The calculated mutual inductance curve is compared with FEA results and measured results in Fig. 7. The calculated, simulated, and measured results agree satisfactorily with each other and prove the validity of the formula. It can be seen that with the increase of the axial distance, the mutual inductance drops quickly to zero and then to negative. The negative value of mutual inductance can be explained by the magnetic flux cancellation theory when the two windings are far away partly overlapped [19]. In the far away partly overlapped state, the magnetic flux generated by the primary winding and secondary winding partly cancels each other, so that their mutual inductance is negative.

The self-inductance of primary and secondary windings can also be measured, and the result is $L_P = L_S = 5.028$ μH. Because L_P and L_S are independent of the axial distance, the M–d curve can be rescaled as a k–d relationship with the transformation from M to k in (33), where k is defined as coupling coefficient

$$k = \sqrt{\frac{M^2}{L_P L_S}}. \tag{33}$$

C. Variation of Air Gap Thickness z

Another test is carried out to investigate the effect of air gap variation. The calculated, simulated, and measured results are given and compared in Fig. 8, where the axial distance is fixed at $d = 9$ mm and the air gap is changed from 2 to 6 mm. The air gap is critical to the mutual coupling between the two windings as well as the performance of the CETSs. The satisfactory agreement among the calculated, simulated, and measured values of the mutual inductance confirms the proposed theory

$$J(r) = \frac{I}{hR \ln(R_2/R_1)}. \tag{34}$$

D. Errors Analysis

In Figs. 5 and 6, some small errors can be found among the inductance values from simulation, calculation, and measurement. Actually, two analytical approximations are made in the derivation of the impedance formula for the purpose of simplification, which may lead to small errors.

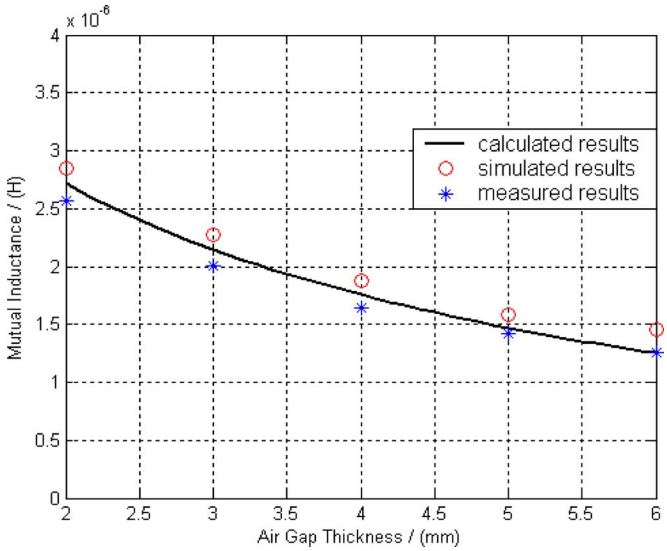

Fig. 8. Mutual inductance as a function of air gap.

1) The first approximation was proposed in [23]. The current density at radius r for a coil current I is given in (34), with an inverse relationship between current density and radius. Since in a trace, the inside path for current flow is shorter than the outside path of the section, it follows that the resistance on the inside is smaller, and therefore, the current density is higher. It is also assumed that the current density variation over the height of the cross section is negligible [23]. However, the current density over the cross-sectional area of the trace is redistributed due to the skin effect and the proximity effect at high frequency, with the trend that the more the intensive magnetic field or the higher the operating frequency is, the more nonuniform the current density becomes. Therefore, the calculation errors are dependent on the operating frequency (f) and the distance between upper and bottom substrates (S in Fig. 2). If the operating frequency is too high or S is very small, the difference between calculated and practical values can become significant. For the charging platform application, in which the typical values of f and S are several hundred kilohertz and several millimeters, respectively, the formula can give an acceptably accurate predication on the inductance. More importantly, it demonstrates the dependence of the mutual inductance variation on the relative position between transmitter and receiver.
2) The analytical model is based on the assumption that the double-layer substrate is infinite in the radial direction. However, in practical measurement, a substrate with a size more than double of the coil is used to simulate the infinite substrate, as mentioned in Section III-A. The air gap effect and the fringing effect due to the finite substrates cannot be totally eliminated in practice. Thus, small errors are observed in Figs. 5 and 6, and they cannot be totally avoided.

IV. Analysis and Discussion

As illustrated in Fig. 7, the " *mutual inductance curve*" drops quickly, with the energy-receiving windings and the energy-transmitting windings moved apart from each other.

TABLE II
Parameters of the Windings Tested in Section III

	Test 1	Test 2	Test 3
N_P, N_S	2, 6, 10, 14	6	6
s_P, s_S	0.8*mm*	0.8*mm*, 1.5*mm*, 2.2*mm*	0.8*mm*
w_P, w_S	0.5*mm*	0.5*mm*	0.5*mm*, 1.0*mm*, 1.5*mm*
R_P, R_S	15*mm*	15*mm*	15*mm*

The detrimental effect of the axial distance on the mutual inductance value is prominent. Therefore, the energy transmission efficiency of contactless charging system decreases dramatically when the axial distance increases. Definitely, a couple of windings whose characteristics can create a relative "smooth" mutual inductance curve must be preferred in contactless charging systems design, in order to reduce the variability of the energy transmission characteristics

For a given footprint area (i.e., the outermost radius is fixed), the flux distribution of a planar spiral winding and the self-inductance highly depend on the winding geometry. These inductive parameters vary with: 1) the number of turns N; 2) conductor width w; and 3) track separation s . Moreover, the mutual inductance curve in Fig. 7 is actually dependent on the flux distribution of primary and secondary windings. The mutual inductance curve is consequently determined by the geometry of contactless planar transformers for a given EM shielding structure. In this section, mutual inductance calculations are performed on a series of contactless planar transformers in order to explore the dependent relationship between the transformer's dimensional parameters and the mutual inductance values. The prototype in Section II will be used in the analysis and discussion.

In this study, the geometries of primary winding and secondary winding are kept identical, and their parameter values have been given in Table I. As shown in Table II, tests are carried out by making one parameter a variable. Mutual inductance between the primary winding and secondary winding is calculated when they are moved from coaxial to partial overlapped, and finally, nonoverlapped state. This means that the displacement of their central axes of the two windings increases from 0 to 30 mm within several steps ($R_P = R_S = 15$ mm).

Test 1 (Different number of turns with the same R, w, and s): The first test is carried out for the windings with different number of turns while keeping their track width and track separation fixed at 0.5 and 0.8 mm, respectively (i.e., test 1 of Table II). The mutual inductance curves as functions of axial distance for the transformers of 2-turns, 6-turns, 10-turns and 14-turns are plotted and compared in Fig. 9. For clear comparison, all the mutual inductance results are normalized with the value when two windings are in coaxial state (i.e., $d = 0$), M_{co}, and the axial distance values are normalized with windings' outermost radius $R = 15$ mm. Therefore, all these curves originate from the point of unity value at the y-axis. Calculated results in Fig. 9 indicate that increasing the windings' number of turns can accelerate the rate of decline of the mutual inductance curve.

Test 2 (Different track separation with the same R, N, and w): A series of contactless planar transformers with different track separation have been tested and examined. The dimensions

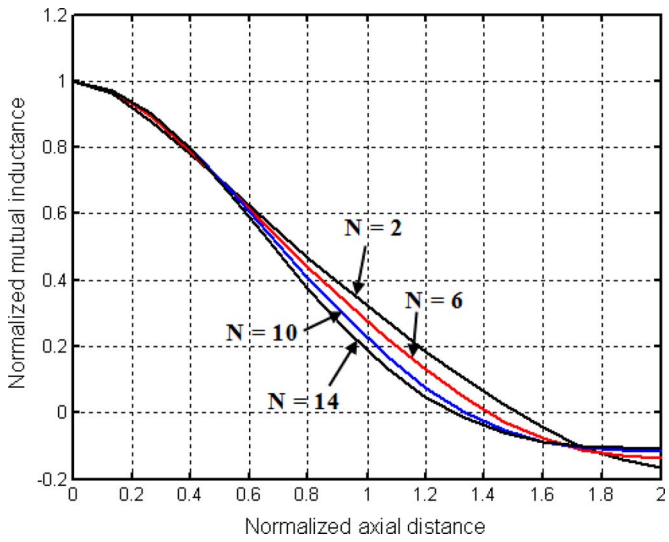

Fig. 9. Mutual inductance as a function of axial distance with different number of turns.

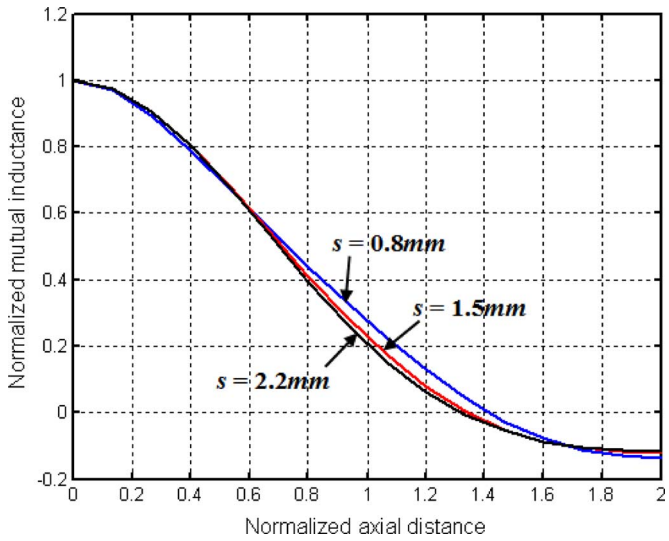

Fig. 10. Mutual inductance as a function of axial distance with different track separation.

of this transformer series are tabulated in the Test 2 column of Table II. The geometry of primary winding is the same as that of the secondary winding, and they are also moved from $d = 0$ mm to $d = 30$ mm. The normalized calculated results of mutual inductance when $s = 0.8$ mm, $s = 1.5$ mm, and $s = 2.2$ mm are plotted in Fig. 10, which indicates that the smoothness of mutual inductance curve can be improved with the track separation decreased.

Test 3 (Different conductor width with the same R, N, and s): This transformer series have different conductor widths but other dimensional parameters are kept constant in this test, as shown in last column of Table II. Fig. 11 shows the normalized mutual inductance as a function of normalized axial distance when $w = 0.5$ mm, $w = 1.0$ mm, and $w = 1.5$ mm. Results from this test show that the rate of decline of the mutual inductance with the axial distance increases with increasing conductor width.

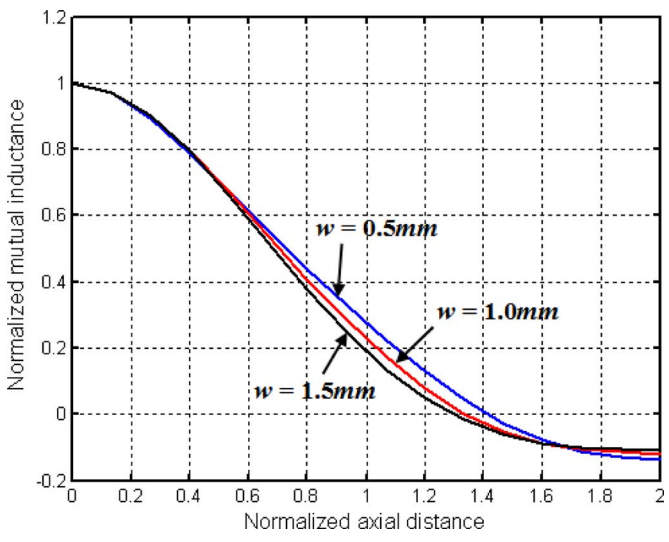

Fig. 11. Mutual inductance as a function of axial distance with different conductor width.

In summary, for these series of planar transformers with identical geometry of primary winding and secondary winding, the path of mutual inductance curve varies with the parameters of N, s, and w. The results in Figs. 9–11 imply that a smoother curve can be obtained from windings having a small number of turns, small track separation, and small conductor width. This is an important observation in the planar winding design. Since the outermost radius in all tests has been fixed, this observation leads to a type of winding that has a much greater value of innermost radius. This means that most of the turns should be placed near the edge of the winding area and not in the central area, resulting in a "hollow" spiral winding. On the contrary, a spiral planar winding with most of the central area covered by copper tracks, like a "full" spiral winding, will have a mutual inductance curve that drops much more quickly. This can be explained by the investigation and comparison about flux distribution of planar spiral windings and concentrated coils [21]. As shown in Fig. 12(a) and (b), the magnetic field of the spiral winding is nonlinear in a "convex" manner that its magnitude is highest in the central region of the spiral winding, while the magnetic field distribution of a coil drops down from the periphery to the center in a "concave" distributed manner. Therefore, the "hollow" spiral winding acts as coils, and thus, creates a "concave" magnetic field, and the "full" spiral winding acts as a fully printed spiral winding, and thus its magnetic field distribution is in a "convex" manner.

V. Conclusion

In this paper, a formula for the mutual inductance calculation for two coaxial or noncoaxial planar spiral windings sandwiched between two double-layer substrates has been established and verified. It can quickly determine the mutual coupling of two planar windings that can have different relative positions and distance between them. This new calculation tool provides a new and useful tool for calculating the mutual inductance of a movable planar coil and the fixed planar coil on the wireless

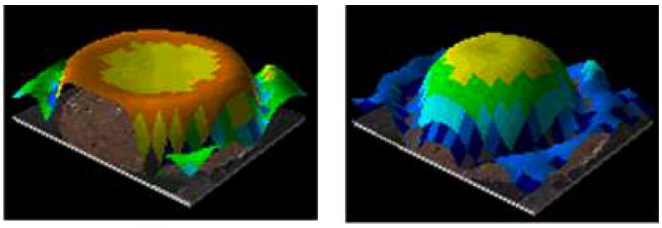

(a) (b)

Fig. 12. Magnetic field intensity scanned by EMC scanner [21]. (a) Coil only. (b) Spiral winding only.

battery charging platform. With the proposed formula, the dependent relationship between the transformer's dimensional parameters and the "mutual inductance curve" is explored. The calculation method can be used to study the characteristic of movable planar winding structures and also coupling effects for loosely coupled winding structures.

REFERENCES

[1] H. Abe, H. Sakamoto, and K. Harada, "A noncontact charger using resonant converter with parallel capacitor of the secondary coil," *IEEE Trans. Ind. Appl.* , vol. 36, no. 2, pp. 444–451, Mar. 2000.

[2] Y. Jang and M. M. Jovanovic, "A contactless electrical energy transmission system for portable-telephone battery chargers ," *IEEE Trans. Ind. Electron.*, vol. 50, no. 3, pp. 520–527, Jun. 2003.

[3] C. G. Kim, D. H. Seo, J. S. You, J. H. Park, and B. H. Cho, "Design of a contactless battery charger for cellular phone," *IEEE Trans. Ind. Electron.* , vol. 48, no. 6, pp. 1238–1247, Dec. 2001.

[4] G. B. Joung and B. H. Cho, " An energy transmission system for an artificial heart using leakage inductance compensation of transcutaneous transformer," *IEEE Trans. Power Electron.*, vol. 13, no. 6 , pp. 1013–1022, Nov. 1998 .

[5] M. Takahashi, K. Watanabe, F. Sato, and H. Matsuki, "Signal transmission system for high frequency magnetic telemetry for an artificial heart," *IEEE Trans. Magn.*, vol. 41, no. 10, pp. 4173–4175, Oct. 2005.

[6] D. W. Baarman, S. J. McPhilliamy, and C. Houghton, "Inductively powered apparatus ," U.S. Patent 7 279 843 Oct. 9, 2007, Access Business Group International LLC.

[7] D. W. Baarman, S. J. McPhilliamy, and C. Houghton, "Inductively powered apparatus ," U.S. Patent 7 233 222 Jun. 19 , 2007, Access Business Group International LLC.

[8] D. W. Baarman, S. J. McPhilliamy, and C. Houghton, "Inductively powered apparatus ," U.S. Patent 7 126 450 Oct. 24 , 2006, Access Business Group International LLC.

[9] D. W. Baarman and T. L. Lautzenheiser, " Inductive coil assembly," U.S. Patent 7 411 479 Aug. 12, 2008, Access Business Group International LLC.

[10] D. W. Baarman and T. L. Lautzenheiser, " Inductive coil assembly," U.S. Patent 7 132 918 Nov. 7, 2006, Access Business Group International LLC.

[11] D. W. Baarman and T. L. Lautzenheiser, " Inductive coil assembly," U.S. Patent 7 116 200 Oct. 3, 2006, Access Business Group International LLC.

[12] D. W. Baarman and T. L. Lautzenheiser, " Inductive coil assembly," U.S. Patent 6 975 198 Dec. 13, 2005, Access Business Group International LLC.

[13] L. Cheng, J. W. Hay, and P. G. Beart, "Portable contact-less power transfer devices and rechargeable batteries," U.S. Patent 7 248 017 Jul. 2007.

[14] A. Sabo, "Alignment independent and self aligning inductive power transfer system ," U.S. Patent 6 803 744 Oct. 2004 .

[15] S. Y. R. Hui, "Inductive battery charger system with primary transformer windings formed in multiplayer structure," U.S. Patent 7 164 255 Jan. 2007.

[16] F. Hsu, "Inductive powering surface for powering portable devices," U.S. Patent 7 262 700 Aug. 2007.

[17] T. Sekitani, M. Takamiya, Y. Noguchi, S. Nakano, Y. Kato, K. Hizu , H. Kawaguchi, T. Sakurai, and T. Someya , "A large-area flexible wireless power transmission sheet using printed plastic MEMS switches and organic field-effect transistors," in *Proc. Int. Electron Devices Meeting (IEDM 2006)*, pp. 1–4.

[18] S. Y. R. Hui and W. C. Ho, " A new generation of universal contactless battery charging platform for portable consumer electronic equipment ," *IEEE Trans. Power Electron.*, vol. 20, no. 3, pp. 620–627, May 2005.

[19] X. Liu and S. Y. R. Hui, "Equivalent circuit modeling of a multilayer planar winding array structure for use in a universal contactless battery charging platform," *IEEE Trans. Power Electron.*, vol. 22, no. 1, pp. 21–29, Jan. 2007.

[20] X. Liu and S. Y. R. Hui, "Simulation study and experimental verification of a universal contactless battery charging platform with localized charging features," *IEEE Trans. Power Electron.*, vol. 22 , no. 6, pp. 2202–2210, Nov. 2007.

[21] X. Liu and S. Y. R. Hui, "Optimal design of a hybrid winding structure for planar contactless battery charging platform ," *IEEE Trans. Power Electron.*, vol. 23, no. 1, pp. 455–463, Jan. 2008.

[22] W. G. Hurley and M. C. Duffy, "Calculation of self and mutual impedances in planar magnetic structures," *IEEE Trans. Magn.*, vol. 31, no. 4, pp. 2416 –2422, Jul. 1995.

[23] W. G. Hurley and M. C. Duffy, "Calculation of self and mutual impedances in planar sandwich inductors," *IEEE Trans. Magn.*, vol. 33, no. 3, pp. 2282 –2290, May 1997.

[24] W. G. Hurley, M. C. Duffy, S. O'Reilly, and S. C. O'Mathuna , "Impedance formulas for planar magnetic structures with spiral windings," *IEEE Trans. Ind. Electron.*, vol. 46, no. 2, pp. 271–278, Apr. 1999 .

[25] W. A. Roshen, "Effect of finite thickness of magnetic substrate on planar inductors ," *IEEE Trans. Magn.*, vol. 26, no. 1, pp. 270–275, Jan. 1990.

[26] W. A. Roshen, "Analysis of planar sandwich inductors by current images ," *IEEE Trans. Magn.*, vol. 26, no. 5, pp. 2880–2887, Sep. 1990.

[27] X. Liu and S. Y. R. Hui, "An analysis of a double-layer electromagnetic shield for a universal contactless battery charging platform," in *Proc. IEEE Power Electron Spec. Conf. (PESC 2005)*, Recife, Brazil, Jun. , pp. 1767 –1772.

[28] Y. P. Su, X. Liu, and S. Y. R. Hui, "Extended theory on the inductance calculation of planar spiral windings including the effect of double-layer electromagnetic shield," *IEEE Trans. Power Electron.*, vol. 23, no. 4, pp. 2052–2061, Jul. 2008.

[29] P. Morse and H. Feshback, *Methods of Theoretical Physics, Part I.* New York: McGraw-Hill , 1953, ch. 6.

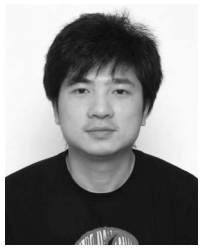

Y. P. Su (S'07) was born in China in 1981. He received the B.S. degree in electrical engineering from Tsinghua University, Beijing, China, in 2005, and the M.Phil. degree from the City University of Hong Kong, Kowloon, Hong Kong, in 2008. He is working toward his Ph.D. degree at Virginia Polytechnic Institute and State University.

He was a Research Associate at the Center for Power Electronics, City University of Hong Kong. His current research interests include planar magnetic components, circuit integration in power electronics, numerical calculation of the electromagnetic field, and electromagnetic compatibility (EMC)/electromagnetic interference (EMI).

Xun Liu (M'07) was born in China in 1978. He received the B.S. and M.S. degrees in electrical engineering from Tsinghua University, Beijing, China, in 2001 and 2003, respectively, and the Ph.D. degree from the City University of Hong Kong, Kowloon, Hong Kong, in 2007.

He is currently a Technology Manager at ConvenientPower (HK), Ltd., Shatin, NT, Hong Kong, where he is engaged in innovation and research of a new generation of universal wireless charging platform for a wide range of consumer electronic products. His current research interests include electromagnetic induction, power magnetics, planar integration in power electronics, applied superconductivity, and electromagnetic compatibility (EMC)/electromagnetic interference (EMI).

S. Y. Ron Hui (M'87–SM'94–F'03) was born in Hong Kong in 1961. He received the B.Sc. degree (with honors) from the University of Birmingham, Birmingham, U.K., in 1984, and the D.I.C. and the Ph.D. degree from the Imperial College of Science and Technology, University of London, London, U.K., in 1987.

From 1987 to 1990, he was a Lecturer of power electronics at the University of Nottingham, Nottingham, U.K. In 1990, he was a Lecturer at the University of Technology, Sydney, N.S.W., Australia, where he became a Senior Lecturer in 1991. In 1993, he joined the University of Sydney, where he was promoted to a Reader of electrical engineering in 1996. From 1999 to 2004, he was the Associate Dean of the Faculty of Science and Engineering at City University of Hong Kong (CityU), Kowloon, Hong Kong. He is currently a Chair Professor of electronic engineering at CityU. He has authored or coauthored more than 200 technical papers, including over 120 refereed journal publications. He holds over 40 patents.

Prof. Hui has been an Associate Editor of the IEEE TRANSACTIONS ON POWER ELECTRONICS and the IEEE TRANSACTIONS ON INDUSTRIAL ELECTRONICS since 1997. Since October 2002, he has been an At-Large Member of the IEEE Power Electronics Society (PELS) AdCom. From 2004 to 2007, he was appointed as an IEEE Distinguished Lecturer by the IEEE PELS. He received the Teaching Excellence Award in 1999 and the Grand Applied Research Excellence Award in 2001 from CityU, and the Best Paper Award from the IEEE Industry Applications Society (IAS) Committee on Production and Applications of Light in 2002.